EUROPEAN ORGANIZATION FOR NUCLEAR RESEARCH

CERN–EP-2001-033

03 May 2001

Single Intermediate Vector Boson Production in e^+e^- collisions at $\sqrt{s} = 183$ and 189 GeV

DELPHI Collaboration

Abstract

The cross-sections for the production of single charged and neutral intermediate vector bosons were measured using integrated luminosities of 52 pb^{-1} and 154 pb^{-1} collected by the DELPHI experiment at centre-of-mass energies of 182.6 GeV and 188.6 GeV, respectively. The cross-sections for the reactions were determined in limited kinematic regions. The results found are in agreement with the Standard Model predictions for these channels.

(Accepted by Phys.Lett.B)

P.Abreu[22], W.Adam[51], T.Adye[37], P.Adzic[12], I.Ajinenko[43], Z.Albrecht[18], T.Alderweireld[2], G.D.Alekseev[17], R.Alemany[9], T.Allmendinger[18], P.P.Allport[23], S.Almehed[25], U.Amaldi[29], N.Amapane[46], S.Amato[48], E.Anashkin[36], E.G.Anassontzis[3], P.Andersson[45], A.Andreazza[28], S.Andringa[22], N.Anjos[22], P.Antilogus[26], W-D.Apel[18], Y.Arnoud[15], B.Åsman[45], J-E.Augustin[24], A.Augustinus[9], P.Baillon[9], A.Ballestrero[46], P.Bambade[9,20], F.Barao[22], G.Barbiellini[47], R.Barbier[26], D.Y.Bardin[17], G.Barker[18], A.Baroncelli[39], M.Battaglia[16], M.Baubillier[24], K-H.Becks[53], M.Begalli[6], A.Behrmann[53], T.Bellunato[9], Yu.Belokopytov[9], N.C.Benekos[32], A.C.Benvenuti[5], C.Berat[15], M.Berggren[24], L.Berntzon[45], D.Bertrand[2], M.Besancon[40], N.Besson[40], M.S.Bilenky[17], D.Bloch[10], H.M.Blom[31], L.Bol[18], M.Bonesini[29], M.Boonekamp[40], P.S.L.Booth[23], G.Borisov[20], C.Bosio[42], O.Botner[49], E.Boudinov[31], B.Bouquet[20], T.J.V.Bowcock[23], I.Boyko[17], I.Bozovic[12], M.Bozzo[14], M.Bracko[44], P.Branchini[39], R.A.Brenner[49], P.Bruckman[9], J-M.Brunet[8], L.Bugge[33], P.Buschmann[53], M.Caccia[28], M.Calvi[29], T.Camporesi[9], V.Canale[38], F.Carena[9], L.Carroll[23], C.Caso[14], M.V.Castillo Gimenez[50], A.Cattai[9], F.R.Cavallo[5], M.Chapkin[43], Ph.Charpentier[9], P.Checchia[36], G.A.Chelkov[17], R.Chierici[46], P.Chliapnikov[9,43], P.Chochula[7], V.Chorowicz[26], J.Chudoba[30], K.Cieslik[19], P.Collins[9], R.Contri[14], E.Cortina[50], G.Cosme[20], F.Cossutti[9], M.Costa[50], H.B.Crawley[1], D.Crennell[37], J.Croix[10], G.Crosetti[14], J.Cuevas Maestro[34], S.Czellar[16], J.D'Hondt[2], J.Dalmau[45], M.Davenport[9], W.Da Silva[24], G.Della Ricca[47], P.Delpierre[27], N.Demaria[46], A.De Angelis[47], W.De Boer[18], C.De Clercq[2], B.De Lotto[47], A.De Min[9], L.De Paula[48], H.Dijkstra[9], L.Di Ciaccio[38], K.Doroba[52], M.Dracos[10], J.Drees[53], M.Dris[32], G.Eigen[4], T.Ekelof[49], M.Ellert[49], M.Elsing[9], J-P.Engel[10], M.Espirito Santo[9], G.Fanourakis[12], D.Fassouliotis[12], M.Feindt[18], J.Fernandez[41], A.Ferrer[50], E.Ferrer-Ribas[20], F.Ferro[14], A.Firestone[1], U.Flagmeyer[53], H.Foeth[9], E.Fokitis[32], F.Fontanelli[14], B.Franek[37], A.G.Frodesen[4], R.Fruhwirth[51], F.Fulda-Quenzer[20], J.Fuster[50], A.Galloni[23], D.Gamba[46], S.Gamblin[20], M.Gandelman[48], C.Garcia[50], C.Gaspar[9], M.Gaspar[48], U.Gasparini[36], Ph.Gavillet[9], E.N.Gazis[32], D.Gele[10], T.Geralis[12], N.Ghodbane[26], I.Gil[50], F.Glege[53], R.Gokieli[9,52], B.Golob[9,44], G.Gomez-Ceballos[41], P.Goncalves[22], I.Gonzalez Caballero[41], G.Gopal[37], L.Gorn[1], Yu.Gouz[43], V.Gracco[14], J.Grahl[1], E.Graziani[39], G.Grosdidier[20], K.Grzelak[52], J.Guy[37], C.Haag[18], F.Hahn[9], S.Hahn[53], S.Haider[9], A.Hallgren[49], K.Hamacher[53], J.Hansen[33], F.J.Harris[35], S.Haug[33], F.Hauler[18], V.Hedberg[9,25], S.Heising[18], J.J.Hernandez[50], P.Herquet[2], H.Herr[9], O.Hertz[18], E.Higon[50], S-O.Holmgren[45], P.J.Holt[35], S.Hoorelbeke[2], M.Houlden[23], J.Hrubec[51], G.J.Hughes[23], K.Hultqvist[9,45], J.N.Jackson[23], R.Jacobsson[9], P.Jalocha[19], Ch.Jarlskog[25], G.Jarlskog[25], P.Jarry[40], B.Jean-Marie[20], D.Jeans[35], E.K.Johansson[45], P.Jonsson[26], C.Joram[9], P.Juillot[10], L.Jungermann[18], F.Kapusta[24], K.Karafasoulis[12], S.Katsanevas[26], E.C.Katsoufis[32], R.Keranen[18], G.Kernel[44], B.P.Kersevan[44], Yu.Khokhlov[43], B.A.Khomenko[17], N.N.Khovanski[17], A.Kiiskinen[16], B.King[23], A.Kinvig[23], N.J.Kjaer[9], O.Klapp[53], P.Kluit[31], P.Kokkinias[12], V.Kostioukhine[43], C.Kourkoumelis[3], O.Kouznetsov[17], M.Krammer[51], E.Kriznic[44], Z.Krumstein[17], P.Kubinec[7], M.Kucharczyk[19], J.Kurowska[52], J.W.Lamsa[1], J-P.Laugier[40], G.Leder[51], F.Ledroit[15], L.Leinonen[45], A.Leisos[12], R.Leitner[30], G.Lenzen[53], V.Lepeltier[20], T.Lesiak[19], M.Lethuillier[26], J.Libby[35], W.Liebig[53], D.Liko[9], A.Lipniacka[45], I.Lippi[36], J.G.Loken[35], J.H.Lopes[48], J.M.Lopez[41], R.Lopez-Fernandez[15], D.Loukas[12], P.Lutz[40], L.Lyons[35], J.MacNaughton[51], J.R.Mahon[6], A.Maio[22], A.Malek[53], S.Maltezos[32], V.Malychev[17], F.Mandl[51], J.Marco[41], R.Marco[41], B.Marechal[48], M.Margoni[36], J-C.Marin[9], C.Mariotti[9], A.Markou[12], C.Martinez-Rivero[9], S.Marti i Garcia[9], J.Masik[13], N.Mastroyiannopoulos[12], F.Matorras[41], C.Matteuzzi[29], G.Matthiae[38], F.Mazzucato[36], M.Mazzucato[36], M.Mc Cubbin[23], R.Mc Kay[1], R.Mc Nulty[23], G.Mc Pherson[23], E.Merle[15], C.Meroni[28], W.T.Meyer[1], A.Miagkov[43], E.Migliore[9], L.Mirabito[26], W.A.Mitaroff[51], U.Mjoernmark[25], T.Moa[45], M.Moch[18], K.Moenig[9,11], M.R.Monge[14], J.Montenegro[31], D.Moraes[48], P.Morettini[14], G.Morton[35], U.Mueller[53], K.Muenich[53], M.Mulders[31], L.M.Mundim[6], W.J.Murray[37], B.Muryn[19], G.Myatt[35], T.Myklebust[33], M.Nassiakou[12], F.L.Navarria[5], K.Nawrocki[52], P.Negri[29], S.Nemecek[13], N.Neufeld[51], R.Nicolaidou[40], P.Niezurawski[52], M.Nikolenko[10,17], V.Nomokonov[16], A.Nygren[25], V.Obraztsov[43], A.G.Olshevski[17], A.Onofre[22], R.Orava[16], K.Osterberg[9], A.Ouraou[40], A.Oyanguren[50], M.Paganoni[29], S.Paiano[5], R.Pain[24], R.Paiva[22], J.Palacios[35], H.Palka[19], Th.D.Papadopoulou[32], L.Pape[9], C.Parkes[9], F.Parodi[14], U.Parzefall[23], A.Passeri[39], O.Passon[53], T.Pavel[25], M.Pegoraro[36], L.Peralta[22], V.Perepelitsa[50], M.Pernicka[51], A.Perrotta[5], C.Petridou[47], A.Petrolini[14], H.T.Phillips[37], F.Pierre[40], M.Pimenta[22], E.Piotto[28], T.Podobnik[44], V.Poireau[40], M.E.Pol[6], G.Polok[19], P.Poropat[47], V.Pozdniakov[17], P.Privitera[38], N.Pukhaeva[17], A.Pullia[29], D.Radojicic[35], S.Ragazzi[29], H.Rahmani[32], P.N.Ratoff[21], A.L.Read[33], P.Rebecchi[9], N.G.Redaelli[29], M.Regler[51], J.Rehn[18], D.Reid[31], R.Reinhardt[53], P.B.Renton[35], L.K.Resvanis[3], F.Richard[20], J.Ridky[13], G.Rinaudo[46], I.Ripp-Baudot[10], A.Romero[46], P.Ronchese[36], E.I.Rosenberg[1], P.Rosinsky[7], P.Roudeau[20], T.Rovelli[5], V.Ruhlmann-Kleider[40], A.Ruiz[41], H.Saarikko[16], Y.Sacquin[40], A.Sadovsky[17], G.Sajot[15], L.Salmi[16], J.Salt[50], D.Sampsonidis[12], M.Sannino[14], A.Savoy-Navarro[24], C.Schwanda[51], Ph.Schwemling[24], B.Schwering[53], U.Schwickerath[18], F.Scuri[47], P.Seager[21], Y.Sedykh[17], A.M.Segar[35], R.Sekulin[37], G.Sette[14], R.C.Shellard[6], M.Siebel[53], L.Simard[40], F.Simonetto[36], A.N.Sisakian[17], G.Smadja[26], N.Smirnov[43], O.Smirnova[25], G.R.Smith[37], A.Sokolov[43], A.Sopczak[18], R.Sosnowski[52], T.Spassov[9], E.Spiriti[39], C.Stanescu[39], M.Stanitzki[18], K.Stevenson[35], A.Stocchi[20], J.Strauss[51], R.Strub[10], B.Stugu[4], M.Szczekowski[52], M.Szeptycka[52], T.Tabarelli[29], A.Taffard[23], F.Tegenfeldt[49], F.Terranova[29], J.Timmermans[31], N.Tinti[5], L.G.Tkatchev[17], M.Tobin[23], S.Todorova[9], B.Tome[22], A.Tonazzo[9], L.Tortora[39], P.Tortosa[50], D.Treille[9], G.Tristram[8], M.Trochimczuk[52], C.Troncon[28], M-L.Turluer[40], I.A.Tyapkin[17], P.Tyapkin[25], S.Tzamarias[12], O.Ullaland[9], V.Uvarov[43], G.Valenti[9,5], E.Vallazza[47], P.Van Dam[31], W.Van den Boeck[2], J.Van Eldik[9,31], A.Van Lysebetten[2], N.van Remortel[2], I.Van Vulpen[31], G.Vegni[28], L.Ventura[36], W.Venus[37,9], F.Verbeure[2], P.Verdier[26],

M.Verlato[36], L.S.Vertogradov[17], V.Verzi[28], D.Vilanova[40], L.Vitale[47], E.Vlasov[43], A.S.Vodopyanov[17], G.Voulgaris[3], V.Vrba[13], H.Wahlen[53], A.J.Washbrook[23], C.Weiser[9], D.Wicke[9], J.H.Wickens[2], G.R.Wilkinson[35], M.Winter[10], M.Witek[19], G.Wolf[9], J.Yi[1], O.Yushchenko[43], A.Zalewska[19], P.Zalewski[52], D.Zavrtanik[44], E.Zevgolatakos[12], N.I.Zimin[17,25], A.Zintchenko[17], Ph.Zoller[10], G.Zumerle[36], M.Zupan[12]

[1]Department of Physics and Astronomy, Iowa State University, Ames IA 50011-3160, USA
[2]Physics Department, Univ. Instelling Antwerpen, Universiteitsplein 1, B-2610 Antwerpen, Belgium
and IIHE, ULB-VUB, Pleinlaan 2, B-1050 Brussels, Belgium
and Faculté des Sciences, Univ. de l'Etat Mons, Av. Maistriau 19, B-7000 Mons, Belgium
[3]Physics Laboratory, University of Athens, Solonos Str. 104, GR-10680 Athens, Greece
[4]Department of Physics, University of Bergen, Allégaten 55, NO-5007 Bergen, Norway
[5]Dipartimento di Fisica, Università di Bologna and INFN, Via Irnerio 46, IT-40126 Bologna, Italy
[6]Centro Brasileiro de Pesquisas Físicas, rua Xavier Sigaud 150, BR-22290 Rio de Janeiro, Brazil
and Depto. de Física, Pont. Univ. Católica, C.P. 38071 BR-22453 Rio de Janeiro, Brazil
and Inst. de Física, Univ. Estadual do Rio de Janeiro, rua São Francisco Xavier 524, Rio de Janeiro, Brazil
[7]Comenius University, Faculty of Mathematics and Physics, Mlynska Dolina, SK-84215 Bratislava, Slovakia
[8]Collège de France, Lab. de Physique Corpusculaire, IN2P3-CNRS, FR-75231 Paris Cedex 05, France
[9]CERN, CH-1211 Geneva 23, Switzerland
[10]Institut de Recherches Subatomiques, IN2P3 - CNRS/ULP - BP20, FR-67037 Strasbourg Cedex, France
[11]Now at DESY-Zeuthen, Platanenallee 6, D-15735 Zeuthen, Germany
[12]Institute of Nuclear Physics, N.C.S.R. Demokritos, P.O. Box 60228, GR-15310 Athens, Greece
[13]FZU, Inst. of Phys. of the C.A.S. High Energy Physics Division, Na Slovance 2, CZ-180 40, Praha 8, Czech Republic
[14]Dipartimento di Fisica, Università di Genova and INFN, Via Dodecaneso 33, IT-16146 Genova, Italy
[15]Institut des Sciences Nucléaires, IN2P3-CNRS, Université de Grenoble 1, FR-38026 Grenoble Cedex, France
[16]Helsinki Institute of Physics, HIP, P.O. Box 9, FI-00014 Helsinki, Finland
[17]Joint Institute for Nuclear Research, Dubna, Head Post Office, P.O. Box 79, RU-101 000 Moscow, Russian Federation
[18]Institut für Experimentelle Kernphysik, Universität Karlsruhe, Postfach 6980, DE-76128 Karlsruhe, Germany
[19]Institute of Nuclear Physics and University of Mining and Metalurgy, Ul. Kawiory 26a, PL-30055 Krakow, Poland
[20]Université de Paris-Sud, Lab. de l'Accélérateur Linéaire, IN2P3-CNRS, Bât. 200, FR-91405 Orsay Cedex, France
[21]School of Physics and Chemistry, University of Lancaster, Lancaster LA1 4YB, UK
[22]LIP, IST, FCUL - Av. Elias Garcia, 14-1^{o}, PT-1000 Lisboa Codex, Portugal
[23]Department of Physics, University of Liverpool, P.O. Box 147, Liverpool L69 3BX, UK
[24]LPNHE, IN2P3-CNRS, Univ. Paris VI et VII, Tour 33 (RdC), 4 place Jussieu, FR-75252 Paris Cedex 05, France
[25]Department of Physics, University of Lund, Sölvegatan 14, SE-223 63 Lund, Sweden
[26]Université Claude Bernard de Lyon, IPNL, IN2P3-CNRS, FR-69622 Villeurbanne Cedex, France
[27]Univ. d'Aix - Marseille II - CPP, IN2P3-CNRS, FR-13288 Marseille Cedex 09, France
[28]Dipartimento di Fisica, Università di Milano and INFN-MILANO, Via Celoria 16, IT-20133 Milan, Italy
[29]Dipartimento di Fisica, Univ. di Milano-Bicocca and INFN-MILANO, Piazza delle Scienze 2, IT-20126 Milan, Italy
[30]IPNP of MFF, Charles Univ., Areal MFF, V Holesovickach 2, CZ-180 00, Praha 8, Czech Republic
[31]NIKHEF, Postbus 41882, NL-1009 DB Amsterdam, The Netherlands
[32]National Technical University, Physics Department, Zografou Campus, GR-15773 Athens, Greece
[33]Physics Department, University of Oslo, Blindern, NO-1000 Oslo 3, Norway
[34]Dpto. Fisica, Univ. Oviedo, Avda. Calvo Sotelo s/n, ES-33007 Oviedo, Spain
[35]Department of Physics, University of Oxford, Keble Road, Oxford OX1 3RH, UK
[36]Dipartimento di Fisica, Università di Padova and INFN, Via Marzolo 8, IT-35131 Padua, Italy
[37]Rutherford Appleton Laboratory, Chilton, Didcot OX11 OQX, UK
[38]Dipartimento di Fisica, Università di Roma II and INFN, Tor Vergata, IT-00173 Rome, Italy
[39]Dipartimento di Fisica, Università di Roma III and INFN, Via della Vasca Navale 84, IT-00146 Rome, Italy
[40]DAPNIA/Service de Physique des Particules, CEA-Saclay, FR-91191 Gif-sur-Yvette Cedex, France
[41]Instituto de Fisica de Cantabria (CSIC-UC), Avda. los Castros s/n, ES-39006 Santander, Spain
[42]Dipartimento di Fisica, Università degli Studi di Roma La Sapienza, Piazzale Aldo Moro 2, IT-00185 Rome, Italy
[43]Inst. for High Energy Physics, Serpukov P.O. Box 35, Protvino, (Moscow Region), Russian Federation
[44]J. Stefan Institute, Jamova 39, SI-1000 Ljubljana, Slovenia and Laboratory for Astroparticle Physics,
Nova Gorica Polytechnic, Kostanjeviska 16a, SI-5000 Nova Gorica, Slovenia,
and Department of Physics, University of Ljubljana, SI-1000 Ljubljana, Slovenia
[45]Fysikum, Stockholm University, Box 6730, SE-113 85 Stockholm, Sweden
[46]Dipartimento di Fisica Sperimentale, Università di Torino and INFN, Via P. Giuria 1, IT-10125 Turin, Italy
[47]Dipartimento di Fisica, Università di Trieste and INFN, Via A. Valerio 2, IT-34127 Trieste, Italy
and Istituto di Fisica, Università di Udine, IT-33100 Udine, Italy
[48]Univ. Federal do Rio de Janeiro, C.P. 68528 Cidade Univ., Ilha do Fundão BR-21945-970 Rio de Janeiro, Brazil
[49]Department of Radiation Sciences, University of Uppsala, P.O. Box 535, SE-751 21 Uppsala, Sweden
[50]IFIC, Valencia-CSIC, and D.F.A.M.N., U. de Valencia, Avda. Dr. Moliner 50, ES-46100 Burjassot (Valencia), Spain
[51]Institut für Hochenergiephysik, Österr. Akad. d. Wissensch., Nikolsdorfergasse 18, AT-1050 Vienna, Austria
[52]Inst. Nuclear Studies and University of Warsaw, Ul. Hoza 69, PL-00681 Warsaw, Poland
[53]Fachbereich Physik, University of Wuppertal, Postfach 100 127, DE-42097 Wuppertal, Germany

1 Introduction

The measurement of the production cross-section of a single vector boson ($e^+e^- \to e^-\bar{\nu}_e W^+$, $e^+e^- \to e^+e^- Z$)[1] is a test of the Standard Model. In addition, the study of these processes is important in the evaluation of background to the search for the Higgs boson and for physics beyond the Standard Model. Single-W production is also interesting in itself for the measurement of the trilinear couplings at the $WW\gamma$ vertex; this measurement, in combination with other physics channels, has been made by the DELPHI Collaboration and is reported elsewhere [1].

This letter presents measurements of single-W and single-Z production cross-sections using the data collected by DELPHI at centre-of-mass energies of 182.6 and 188.6 GeV. The corresponding integrated luminosities are 52 and 154 pb^{-1}, respectively.

The criteria for the selection of the events are mainly based on the information from the tracking system, the calorimeters and the muon chambers of the DELPHI detector. A detailed description of the DELPHI apparatus and its performances can be found in [2,3]. The detector has remained essentially unchanged in the past few years, except for upgrades of the Vertex Detector [4].

2 Definition of the signal

Single boson production is investigated in this paper through four-fermions final states, $e^-\bar{\nu}_e f\bar{f}'$ and $e^+e^- f\bar{f}$. These final states receive contributions from single resonant diagrams producing, respectively, the W and Z signals studied here, and from other diagrams, including doubly resonant production, conversion diagrams and multiperipheral processes [5]. To enhance the single boson production contribution, the cross-sections correspond to the limited kinematic regions described below. The measured cross-sections therefore refer to the entire set of diagrams contributing to the specific final states, with the exception of multiperipheral diagrams [5] whose contributions were evaluated separately and then subtracted.

***$e\nu_e W$* channel:** The four-fermion final states $e^-\bar{\nu}_e q\bar{q}'$ and $e^-\bar{\nu}_e l^+\nu_l$ ($l = \mu, \tau$) can be produced both via single-W production, referred to as $e\nu_e W$ in the following, or via W-pair production. A distinctive feature of $e\nu_e W$ is the fact that the distribution of the electron direction is strongly peaked at small polar angles with respect to the incoming electron beam direction. The signal definition was restricted to the region of phase space where the contribution of the single-W process is dominant. The polar angle of the outgoing electron, θ_{e^-}, was required to be smaller than the lower edge of the DELPHI detector acceptance:

$$|\cos\theta_{e^-}| > 0.9993. \tag{1}$$

Additional selections were applied to avoid the phase space regions of low $f\bar{f}'$ invariant mass, mostly due to multiperipheral diagrams, where large uncertainties affect the cross-section computation. It was required that:

$$\begin{aligned} m_{q\bar{q}'} &> 45 \text{ GeV}/c^2 \quad \text{for} \quad e^-\bar{\nu}_e q\bar{q}', \\ E_{l^+} &> 15 \text{ GeV} \quad \text{for} \quad e^-\bar{\nu}_e l^+\nu_l \ \ (l^+ = \mu^+, \tau^+), \end{aligned} \tag{2}$$

where $m_{q\bar{q}'}$ is the $q\bar{q}'$ invariant mass and E_{l^+} the lepton energy.

[1] Charge conjugate states are implied throughout the text.

Single-W production accounts for more than 90% of all $e^-\bar{\nu}_e q\bar{q}'$ and $e^-\bar{\nu}_e l^+\nu_l$ events in the kinematic region defined above. The sum of the cross-sections in the channels $e^-\bar{\nu}_e q\bar{q}'$, $e^-\bar{\nu}_e\mu^+\nu_\mu$, $e^-\bar{\nu}_e\tau^+\nu_\tau$, hereafter called $e\nu f\bar{f}'$, is then compared to the theoretical calculations from GRC4F [6] and WPHACT [7].

The $e^-\bar{\nu}_e e^+\nu_e$ contributions are treated separately (below) because they have t-channel contributions both for single-W and single-Z topologies which are not easily disentangled.

***eνeν* channel:** In the kinematic region defined above, this final state receives, besides single-W production, a large contribution from Ze^+e^- production (with $Z \to \nu_e\bar{\nu}_e$) and from the interference between single-W and Ze^+e^- processes. In addition it is not possible, experimentally, to disentangle the $e^+\nu_e e^-\bar{\nu}_e$ final state from the $e^+e^-\nu_\mu\bar{\nu}_\mu$ and $e^+e^-\nu_\tau\bar{\nu}_\tau$ final states with the neutrinos produced in $Z \to \nu_\mu\bar{\nu}_\mu, \nu_\tau\bar{\nu}_\tau$ decays. Therefore, a topological cross-section was defined corresponding to the $e\nu e\nu$ final state (where a sum over all neutrino flavours is implied), to be compared with theoretical calculations. This was done restricting further the signal phase space to:

$$|\cos\theta_{e^+}| < 0.72, \qquad E_{e^+} > 30 \text{ GeV}. \tag{3}$$

γ^*/Zee channel: The neutral bosons are produced in the so-called electroweak Compton scattering process $e\gamma \to e\gamma^*/Z$, where a quasi-real photon is radiated from one of the beam electrons and scattered off the other beam [8]. In this paper only decays of the γ^*/Z into hadrons and $\mu^+\mu^-$ pairs have been considered: the signature of such events is an electron, typically of low energy, recoiling against the γ^*/Z system, with the other electron usually lost in the beam-pipe. The signal cross-section presented in this note refers to the overall set of graphs contributing to the $e^+e^-f\bar{f}$ ($f = q, \mu$) final state with the exception of the so-called multiperipheral ones, typical of the $\gamma\gamma$ physics [5]. The signal was defined topologically, requiring at least one electron (tag electron) to be within the acceptance of the DELPHI forward electromagnetic calorimeter, i.e. $|\cos\theta_{e^+}| < 0.985$, and having an energy $E_{e^+} > 4$ GeV. The measured cross-section was then compared with that obtained from the GRC4F program. A selection on the minimum energy of this visible electron, $E_{e^+} > 1$ GeV, was used in the computation of the cross-section to avoid numerical instabilities in the integration.

For both the $e\nu_e W$ and Zee samples, signal events were simulated with the GRC4F event generator. For background processes, different generators were used: EXCALIBUR [9] for the WW and other four-fermion final states, PYTHIA [10] for $q\bar{q}(\gamma)$, TEEGG [11] and BHWIDE [12] for $e^+e^- \to e^+e^-\gamma$, KORALZ [13] for $e^+e^- \to \mu^+\mu^-(\gamma), \tau^+\tau^-(\gamma)$, TWOGAM [14] and BDK [15] for two-photon collisions. All the events were processed through the full DELPHI detector simulation and analysis chain [3].

3 Single-W analysis

Both the hadronic and the leptonic final states were considered in the single-W analysis. They are characterized by the presence of two hadronic jets acoplanar with the beam or by a single lepton with large transverse momentum, respectively [16].

3.1 Selection of hadronic events

The experimental signature of $e^-\bar{\nu}_e q\bar{q}'$ events consists of a pair of acoplanar jets. The undetected neutrino results in a large missing momentum at large angle to the beam direction.

Other physics processes which can give rise to a similar topology are $e^+e^- \to Z\gamma$ with $Z \to q\bar{q}$, WW events with at least one W decaying into hadrons, other four-fermion final states ($l^+l^-q\bar{q}$, $\nu\bar{\nu}q\bar{q}$, the latter being topologically identical to the signal) and two-photon collisions. Some of these processes have cross-sections larger than that of the signal by several orders of magnitude. Sequential cuts on the event variables have been applied to reject them.

A sample of hadronic events was preselected by requiring at least seven charged particles to be measured in the detector. The contribution from two-photon collisions was reduced by requiring the opening angle of the cone around the beam axis which contains 15% of the visible energy to be larger than 18°: $\gamma\gamma$ events are concentrated in the forward regions and have low values of this variable. Furthermore, the total transverse momentum was required to be larger than 16% of $\sqrt{s}$.

The background from $e^+e^- \to q\bar{q}(\gamma)$ was rejected by requiring the effective collision energy, $\sqrt{s'}$ [17], to be smaller than $0.85\sqrt{s}$ and the cosine of the polar angle of the missing momentum to satisfy the condition $|\cos\theta_{miss}| < 0.9$. In addition, since the background is concentrated simultaneously at large $|\cos\theta_{miss}|$ and at values of $\sqrt{s'}$ close to the Z mass, a selection on the correlation of the two variables was applied: $\sqrt{s'} > 160 \cdot |\cos\theta_{miss}| - 30$ GeV. $Z(\gamma)$ events in which the ISR photon escaped undetected in the dead region between the barrel and end-cap electromagnetic calorimeters ($\theta \sim 40°$) were suppressed by looking for signals in the hermeticity counters in a cone of 30° around the direction of the missing momentum.

In addition, a combined selection in the transverse momentum versus visible energy plane was also applied to separate the $e^-\bar{\nu}_e q\bar{q}'$ signal from the WW, $\nu\bar{\nu}q\bar{q}$ and $Z\gamma$ backgrounds. Finally, the planarity of the three-body final state $q\bar{q}\gamma$ was exploited: two jets were reconstructed with all the detected particles, and their acoplanarity[2] was required to exceed 15°.

The most important remaining contribution to the background is from W-pair production. Events in which both W bosons decay into a $q\bar{q}'$ pair tend to have a four-jet topology, and were rejected by requiring the distance parameter for the transition from 3 to 4 jets in the Durham algorithm [18], $D_{3\to4}^{join}$, to be larger than 0.005. When one W decays into $q\bar{q}'$ and the other one into $l\bar{\nu}_\ell$, an isolated lepton with high energy is usually visible: events were rejected if an identified electron or muon was found with an energy larger than 15 GeV and forming an angle of more than 10° with the nearest track. If the lepton is a τ, the topology can be 3-jet-like: the $D_{2\to3}^{join}$ for the transition from 2 to 3 jets was required to exceed 0.05. The residual contamination from $q\bar{q}'\tau\bar{\nu}_\tau$ events in which the τ decay products have very low energy or are very close to one of the hadronic jets was reduced by a selection on the maximum transverse momentum of any particle with respect to the closest jet, $P_{tr}^{max} < 3.5$ GeV/c, as shown in Figure 1.

Table 1 shows the number of selected events in the data at 189 GeV in comparison to the expectation from the Monte Carlo simulation at successive stages of the analysis. As can be seen from Table 1, the main contamination in the final selected sample is due to WW production, with one W decaying into hadrons and the other one into $\tau\bar{\nu}_\tau$.

[2]The acoplanarity was defined as the complementary to 180° of the angle between the projections of the two jet directions in the plane transverse to the beam axis.

	$e\nu_e W$	WW	$Z\gamma$	$\nu\bar{\nu}q\bar{q}$	Others	Total MC	Data
Step 1.	36.3	1392.7	9484.2	29.5	263.8	11206.5	11550
Step 2.	22.6	565.1	503.5	17.3	18.7	1127.2	1130
Step 3.	21.6	146.8	239.0	16.3	15.5	439.2	405
Step 4.	14.1 ± 0.7	21.7 ± 0.9	5.1 ± 0.3	8.9 ± 0.2	0.5 ± 0.5	50.3 ± 1.3	52

Table 1: Number of events expected from the contribution of different channels and observed in the data at different stages of the $e\nu_e W$, $W \to q\bar{q}'$ selection at $\sqrt{s} = 189$ GeV. The column labelled "Others" includes $l^+l^-q\bar{q}$ final states and two-photon collisions. Step 1 = after hadronic preselection and anti-$\gamma\gamma$ cuts; Step 2 = after cuts on $\sqrt{s'}$, $|\cos\theta_{miss}|$ and signal in the hermeticity counters; Step 3 = after the cuts on transverse momentum versus visible energy and on acoplanarity; Step 4 = the final sample after WW rejection. Details on the selection are provided in Section 3.1.

$\sqrt{s}$ (GeV)	Efficiency (%)	σ_{bgd} (pb)	$\mathcal{L}_{int}$ (pb^{-1})	N_{data}	$\sigma_{e^-\bar{\nu}_e q\bar{q}'}$ (pb)
182.6	33.0 ± 1.5	0.224 ± 0.009	51.85	15	$0.20^{+0.25}_{-0.20}$
188.6	28.1 ± 1.2	0.245 ± 0.007	154.00	52	$0.33^{+0.18}_{-0.16}$

Table 2: Performance of the $e^-\bar{\nu}_e q\bar{q}'$ event selection at the two centre-of-mass energies considered in the analysis.

The efficiency of the selection for the signal, the expected background, the luminosity and the number of selected events in the data at the two centre-of-mass energies are reported in Table 2, together with the evaluated cross-section for the hadronic channel alone.

3.2 Selection of leptonic events

The experimental signature of the leptonic channel $e^+e^- \to e^-\bar{\nu}_e l^+\nu_l$ is the presence of a high energy lepton accompanied by a large missing momentum and no other significant energy deposition in the detector. The analysis was optimised for final state leptons that are electrons or muons. In both channels, the contribution from $e^-\bar{\nu}_e\tau^+\nu_\tau$ events was considered as part of the background.

The main backgrounds for the leptonic channel are the radiative production of two leptons $e^+e^- \to l^+l^-(\gamma)$, $e^+e^- \to W^+W^-$ events and two-photon collisions.

Events were selected if exactly one well measured charged particle was reconstructed. The quality of the track measurement was assessed as follows:

- relative error on the momentum, $\Delta p/p$, smaller than 100%;
- track length greater than 20 cm;
- polar angle θ between 10° and 170°;
- impact parameter in the transverse plane, $|IP_{R\phi}|$, smaller than 4 cm, and that along the beam direction, $|IP_z|$, smaller than 3 cm $/ \sin\theta$.

$\sqrt{s}$ (GeV)	Eff. on μ (%)	σ_{bkg} (pb)	$\mathcal{L}_{int}$ (pb^{-1})	N_{data}	$\sigma_{e\nu\mu\nu}$ (pb)
$l = \mu$ 182.6	70.8 ± 1.0	0.013 ± 0.002	51.85	6	$0.147^{+0.076}_{-0.058}$
188.6	63.1 ± 1.0	0.012 ± 0.002	153.45	8	$0.062^{+0.033}_{-0.026}$
$\sqrt{s}$ (GeV)	Eff. on e (%)	σ_{bkg} (pb)	$\mathcal{L}_{int}$ (pb^{-1})	N_{data}	$\sigma_{e\nu e\nu}$ (pb)
$l = e$ 182.6	83.4 ± 3.2	0.038 ± 0.008	51.85	3	$0.024^{+0.048}_{-0.024}$
188.6	81.1 ± 0.9	0.043 ± 0.008	153.45	12	$0.044^{+0.031}_{-0.026}$

Table 3: Performance of the $e^-\bar{\nu}_e\mu^+\nu_\mu$ and $e\nu e\nu$ event selection at the two centre-of-mass energies considered in the analysis.

Loose identification criteria were applied, requiring associated hits in the muon chambers or a significant energy deposition in the electromagnetic calorimeter. For electrons, the acceptance was restricted to the barrel region, $|\cos\theta| < 0.72$, and the best determination of the electron energy was estimated by combining the momentum measurement from the tracking devices and the calorimetric energy. Any other energy deposit in the detector not related to the lepton candidate was required not to exceed 2 GeV. In addition, the presence of tracks not fulfilling the quality criteria listed above was used to veto the event. The acceptance was restricted to the kinematic region of W decays by requiring the lepton momentum to lie below 45% of $\sqrt{s}$ and its transverse momentum to exceed 12% of $\sqrt{s}$.

A large residual contamination was still present, due to cosmic ray events in the muon channel and to Compton scattering in the electron channel. The former were suppressed by tightening the selections on the track impact parameters to $|IP_{R\phi}| < 0.2$ cm and $|IP_z| < 2$ cm for the muons. Compton events can mimic the $W^+ \to e^+\nu_e$ signal when the photon balancing the electron in the transverse plane is lost in the dead region between the barrel and forward electromagnetic calorimeters. Therefore events were rejected if a signal was found in the hermeticity counters at an azimuthal angle larger than 90° from the electron.

Figure 2 shows the momentum distribution of single leptons in data and simulation at 189 GeV. The performance of the analysis at the two centre-of-mass energy values and the results obtained are reported in Table 3.

3.3 Study of systematic uncertainties

The main source of systematic error is the limited simulation statistics, both for the signal and for the background. However this has little influence on the accuracy of the measurement, since the error is dominated by the real data statistics.

Possible inaccuracies in the modelling of background processes were evaluated by comparing different Monte Carlo generators. The only notable effect was found in the $q\bar{q}(\gamma)$ channel, where the background estimate to the hadronic selection evaluated with the ARIADNE [19] event generator was found to be 6.0 ± 0.6 events at 189 GeV. The difference from the value obtained from the PYTHIA samples (5.1 ± 0.3, see Table 1) was considered as a systematic uncertainty.

The total systematic error on the background cross-section, mainly due to the effects listed above, amounts approximately to ±5% in the $q\bar{q}'$ channel and to ±20% in each

Systematic effect	Error on $\sigma_{e\nu f\bar{f}'}$ (pb)	Error on $\sigma_{e\nu e\nu}$ (pb)
$\Delta\sigma_{bkg}$ $(e^-\bar{\nu}_e q\bar{q}')$ $\pm 5\%$	0.041	-
$\Delta\sigma_{bkg}$ $(e\nu e\nu)$ $\pm 20\%$	-	0.0106
$\Delta\sigma_{bkg}$ $(e^-\bar{\nu}_e\mu^+\nu_\mu)$ $\pm 20\%$	0.004	-
$\Delta\varepsilon$ $(e^-\bar{\nu}_e q\bar{q}')$ due to simul. stat.	0.014	-
$\Delta\varepsilon$ $(e^-\bar{\nu}_e l^+\nu_l)$ due to simul. stat	0.001	0.0005
$\Delta\varepsilon$ $(e^-\bar{\nu}_e l^+\nu_l)$ due to ε_{track}	0.001	0.0002
Luminosity $\pm 0.6\%$	0.008	0.0006
Total	0.044	0.0106

Table 4: Contributions to the systematic uncertainty on the $e\nu f\bar{f}'$ and $e\nu e\nu$ cross-sections at $\sqrt{s} = 189$ GeV.

of the leptonic channels (see Tables 2 and 3, for the part due only to the Monte Carlo statistics).

From a comparison of dimuon events in data and simulation, the tracking efficiency, ε_{track}, of DELPHI was found to be overestimated by 0.5% in the simulation. This difference was assumed as systematic error. This has a negligible effect on the background, while it affects the selection efficiency of the signal for leptonic decays of the W.

The luminosity is known with a total error of $\pm 0.6\%$.

The effect of the uncertainties listed above on the measurement of the $e\nu f\bar{f}'$ and $e\nu e\nu$ cross-sections at $\sqrt{s}$=189 GeV are given in Table 4. The total systematic error, obtained from the sum in quadrature of the individual contributions, is at the level of $\pm 10\%$ for $e^-\bar{\nu}_e q\bar{q}'$ and about $\pm 25\%$ in the case of $e\nu e\nu$. For the measurement at 183 GeV, the same relative error was assumed.

4 Single-Z analysis

In the single γ^*/Z analysis, decays of the vector boson into hadronic and $\mu^+\mu^-$ final states were considered. Both final states are characterized by an electron scattered at large angle with respect to the incoming direction. The other electron, lost in the beam pipe, results in a missing momentum pointing along the beam line direction. Instead of attempting to separate the $\gamma^* ee$ from the Zee contributions it was preferred, like in [20], to determine the cross-sections in two separate ranges of the invariant mass, $m_{f\bar{f}}$, of the final system: from 15 to 60 GeV/c^2 and above 60 GeV/c^2. The value of 60 GeV/c^2 was chosen as it represents about the minimum of the differential $m_{f\bar{f}}$ distribution.

4.1 Selection of hadronic events

The experimental signature of these events consists of a pair of jets produced in the hadronic decay of the γ^*/Z recoiling against an electron. To maximize the sensitivity of the analysis in the widest possible range of invariant masses of the γ^*/Z, the event selection was performed in three steps:

1. a loose preselection of hadronic events;
2. the identification of an isolated electron;

	γ^*/Zee	WW	$Z(\gamma)$	$\gamma\gamma$	Others	Total MC	Data
Preselection	179.9	1046.7	3156.5	887.6	103.3	5374.0	5812
e ident.	95.7	118.3	64.0	126.5	4.5	409.0	400
Signal selection	37.3 ± 2.5	3.2 ± 0.4	7.0 ± 0.6	6.9 ± 2.1	0.4 ± 0.1	54.8 ± 3.3	51

Table 5: Number of events expected from the contribution of different channels and observed in the data at different stages of the γ^*/Zee selection at $\sqrt{s} = 189$ GeV in the hadronic channel. The number of expected γ^*/Zee events has been computed using a simulation sample generated with GRC4F. The column labelled "Others" includes Bhabha events and other four-fermion processes, namely $e\nu_e W$ and γ^*/Zee with fully leptonic final state. Details on the selection are provided in Section 4.1.

3. the final selection of signal events, optimized differently in two ranges of the invariant mass of the hadronic system, $m_{q\bar{q}}$, according to the most relevant background process in each region.

The preselection of hadronic events consisted of the following requirements:

- at least five charged particles in the event with at least one in the Time Projection Chamber, the main DELPHI tracking detector, with a measured transverse momentum larger than 2.5 GeV/c;
- in events with more than one electromagnetic shower, the energy of the second most energetic one was required to be less than $0.6E_{beam}$ in order to reject Bhabha events.

The electron candidates were selected by requiring energy depositions in the calorimeter $E_e > 4$ GeV, with an associated charged particle and in the angular acceptance $|\cos\theta_e| < 0.985$. Moreover they had to satisfy the following isolation criteria:

- their angle, α, with respect to the closest particle with momentum $p > 0.5$ GeV/c had to lie in the range $15^\circ < \alpha < 170^\circ$;
- their angle with respect to the second closest particle, with $p > 0.5$ GeV/c, had to be greater than 40°.

Electrons from conversions or from decays were further reduced by requiring their impact parameters with respect to the primary interaction vertex to be $|IP_{R\phi}| < 0.35$ cm in the transverse plane and $|IP_z| < 1$ cm along the beam line.

The charged and neutral particles were then clustered into two jets with the Durham algorithm, excluding the tag electron and rejecting events for which $D_{3\to2}^{join} < 10^{-4}$. A kinematic fit of the event was then performed assuming a topology of signal events with two jets, a visible electron and one lost along the beam line. The four-momentum of the invisible electron was chosen to be $(0, 0, Q_e E, E)$ with Q_e the charge of the tagged electron[3]. Fits with a χ^2 probability smaller than 10^{-5} were rejected.

The final selection of signal events was then performed using the variables after the constrained fit. It was required that:

- $Q_e \cos\theta_e > -0.8$ with θ_e being the polar angle of the tagged electron;
- $Q_e \cos\theta_j^{max} < 0$ with θ_j^{max} being the polar angle of the jet closest to the beam line.

Two different sets of cuts were then applied in distinct regions of $m_{q\bar{q}}$.
For $m_{q\bar{q}} < 60$ GeV/c^2, where the dominant background consisted of two-photon events:

[3]The DELPHI reference frame has the z axis oriented along the incoming e^- beam.

$\sqrt{s}$ (GeV)	$\gamma^*/Z \to q\bar{q}$ mass range (GeV/c^2)	Eff. (%)	σ_{bgd} (pb)	$\mathcal{L}_{int}$ (pb^{-1})	N_{data}	σ (pb)
182.6	$15 < m_{q\bar{q}} < 60$	19.2 ± 2.0	0.05 ± 0.01	51.9	6	$0.33^{+0.28}_{-0.21}$
	$m_{q\bar{q}} > 60$	14.2 ± 1.2	0.05 ± 0.01	51.9	15	$1.66^{+0.57}_{-0.48}$
188.6	$15 < m_{q\bar{q}} < 60$	20.1 ± 2.1	0.05 ± 0.01	154.3	20	$0.41^{+0.16}_{-0.13}$
	$m_{q\bar{q}} > 60$	16.9 ± 1.3	0.07 ± 0.01	154.3	31	$0.79^{+0.23}_{-0.20}$
$\sqrt{s}$ (GeV)	$\gamma^*/Z \to \mu^+\mu^-$ mass range (GeV/c^2)	Eff. (%)	σ_{bgd} (pb)	$\mathcal{L}_{int}$ (pb^{-1})	N_{data}	σ (pb)
182.6	$15 < m_{\mu^+\mu^-} < 60$	5.4 ± 0.3	0.004 ± 0.002	51.9	0	-
	$m_{\mu^+\mu^-} > 60$	33.8 ± 1.5	0.004 ± 0.001	51.9	1	-
188.6	$15 < m_{\mu^+\mu^-} < 60$	5.4 ± 0.3	0.004 ± 0.002	154.3	2	$0.154^{+0.206}_{-0.129}$
	$m_{\mu^+\mu^-} > 60$	33.8 ± 1.5	0.005 ± 0.002	154.3	5	$0.080^{+0.048}_{-0.036}$

Table 6: Performance of the γ^*/Zee event selection at the two centre-of-mass energies considered in the analysis.

- $\cos\alpha^*_{q\bar{q}} > -0.9$ with $\alpha^*_{q\bar{q}}$ being the angle between the two jets in the electron-γ^*/Z rest frame;
- $Q_e \cos\theta_e < 0.9$ or $E_e < 0.75 E_{beam}$.

For $m_{q\bar{q}} > 60$ GeV/c^2, where the dominant background consisted of WW events:

- $Q_e \cos\theta_{miss} > 0.95$ with θ_{miss} being the polar angle of the missing momentum computed before the kinematic fit;
- $Q_e \cos\theta_j^{max} > -0.985$.

The distributions of these variables after the electron identification cuts are shown in Figure 3 for the real and simulated data. The numbers of selected events in the data and the expected contributions from the different backgrounds after each selection step are shown in Table 5.

The efficiency of the selection on the signal, the expected background and the number of selected events in the data at the two centre-of-mass energies are reported in Table 6, together with the evaluated cross-section. The distribution of the invariant mass of the hadronic system and the energy spectrum of the tag electron after the kinematic fit are shown in Figure 4. The peak in the invariant mass distribution around the Z mass corresponds to events for which the contribution of the Zee process is dominant.

4.2 Selection of leptonic events

The search was restricted to events with γ^*/Z going into a $\mu^+\mu^-$ pair. The general features are exactly the same as for the hadronic channel with jets replaced by muons. Thus a three-track signature, of two high momentum muons and one e^+ or e^-, scattered at large angle, is expected in the detector. After a common preselection and lepton identification, the analysis was tuned separately for two kinematic regions: $m_{\mu^+\mu^-} >$ 60 GeV/c^2 and $15 < m_{\mu^+\mu^-} < 60$ GeV/c^2. The signal selection criteria on angular distributions were similar to those used in the hadronic channel.

In the preselection the event was required to have exactly three tracks fulfilling the following criteria:

	γ^*/Zee	$\gamma\gamma \to \mu^+\mu^-$	Others	Total MC	Data
Preselection	5.9 ± 0.1	23.2 ± 1.4	4.5 ± 0.7	33.6 ± 1.6	35
Final selection	2.73 ± 0.10	1.25 ± 0.32	0.14 ± 0.12	4.12 ± 0.36	7

Table 7: Number of events expected from the contribution of different channels and observed in the data at different stages of the γ^*/Zee selection at $\sqrt{s} = 189$ GeV in the leptonic channel. The column "Others" shows the numbers for two or four fermion background processes excluding $\gamma\gamma \to \mu^+\mu^-$.

- fractional error on the momentum $\Delta p/p < 50\%$,
- impact parameter in the transverse plane $|IP_{R\phi}| < 0.5$ cm and along the beam direction $|IP_z| < 3$ cm;
- at least one associated hit in the Vertex Detector.

The sum of the charges of the three particles was required to be ± 1. Possible photon conversions were removed according to the standard DELPHI procedure described in [3]. The minimum opening angle of any track pair had to be larger than 5°.

Since the event topology is clean, the particle identification required at least two tracks to be identified as leptons (μ or e) and at least one of them to be a muon. The momentum of the electron had to be greater than 4 GeV/c. For muon identification the loose criteria were applied as in the case of single-W production (see Section 3.2). The flavour of the possible unidentified track was inferred from partial information taking into account the combination of the charges of the observed particles. In the case of $\mu^+x^-e^\pm$ or $x^+\mu^-e^\pm$, the unidentified track x was treated as μ. For $\mu^+\mu^-x^\pm$ the track x was taken as $e^\pm$. In this way the loss of efficiency due to electron identification was minimal.

The data reduction factor of the preselection was large. At $\sqrt{s} = 189$ GeV, 35 events were preselected with 33.6 ± 1.6 events expected. At this stage the majority of events came from the $\gamma\gamma \to \mu^+\mu^-$ process (see Table 7). The other non-zero contributions came from the following sources (ordered by decreasing significance) : $e^+e^- \to \mu^+\mu^-(\gamma)$, $e^+e^- \to ZZ$, $e^+e^- \to l_1^+l_1^-l_2^+l_2^-$ $(l_1, l_2 = e, \mu, \tau)$, $\gamma^*/Ze^+e^- \to \tau^+\tau^-e^+e^-$, $e^+e^- \to W^+W^-$ and $e^+e^- \to \mu^+\mu^-q\bar{q}$.

The final selection of signal events was similar for the two $m_{\mu^+\mu^-}$ ranges. The allowed angular ranges for the direction of the Z/γ^* momentum and missing momentum were defined by the following conditions, in which Q_e represents the charge of the observed electron:

- $Q_e \cos\theta_{\mu^+\mu^-} > -0.8$ with $\theta_{\mu^+\mu^-}$ being the polar angle of the $\mu^+\mu^-$ system
- $Q_e \cos\theta_{miss} > 0.8$ with θ_{miss} being the polar angle of the missing momentum.

The final selection was dependent on the $\mu^+\mu^-$ invariant mass:

- $Q_e \cos\theta_e > -0.8$ for $m_{\mu^+\mu^-}$ greater than 60 GeV/c^2
- $Q_e \cos\theta_e > -0.7$ for $m_{\mu^+\mu^-}$ between 15 and 60 GeV/c^2.

The stronger condition for the low invariant mass region was to reduce the background from the $\gamma\gamma \to \mu^+\mu^-$ process further. The sum of all other sources such as two- or four-fermion production is an order of magnitude smaller after the final selection.

At 183 GeV in the high invariant mass $m_{\mu^+\mu^-}$ region, one event was found in the data with 0.8 ± 0.1 event expected. For the low mass region no event was observed in the data and 0.6 ± 0.1 event was expected. Due to the low statistics, the value of the cross-section

Systematic effect	Error on σ (pb)	
	$15 < m_{q\bar{q}} < 60$ GeV/c^2	$m_{q\bar{q}} > 60$ GeV/c^2
$\Delta\varepsilon_e$	0.034	0.064
$\Delta\sigma_{bkg}$ $(\gamma\gamma)$ $\pm 20\%$	0.030	0.015
$\Delta\varepsilon$ due to simul. stat	0.043	0.060
$\Delta\sigma_{bkg}$ due to simul. stat.	0.058	0.051
Luminosity $\pm 0.6\%$	0.003	0.005
Total	0.085	0.103

Table 8: Contributions to the systematic uncertainty on the γ^*/Zee cross-sections in the hadronic channel, in the two ranges of invariant mass of the hadronic system, at $\sqrt{s} = 189$ GeV.

Systematic effect	Error on σ (pb)	
	$15 < m_{\mu^+\mu^-} < 60$ GeV/c^2	$m_{\mu^+\mu^-} > 60$ GeV/c^2
$\Delta\sigma_{bkg}$ $(\gamma\gamma)$ $\pm 20\%$	0.016	0.003
$\Delta\varepsilon$ due to simul. stat	0.010	0.004
$\Delta\sigma_{bkg}$ due to simul. stat.	0.028	0.005
Luminosity $\pm 0.6\%$	0.001	0.001
Total	0.034	0.007

Table 9: Contributions to the systematic uncertainty on the γ^*/Zee cross-sections in the leptonic channel, in the two ranges of invariant mass of the $\mu^+\mu^-$ system, at $\sqrt{s} = 189$ GeV.

was not derived. At 189 GeV, where the integrated luminosity was three times greater, 5 events (2.5 ± 0.3 predicted) and 2 events (1.6 ± 0.2 predicted) were selected in the high and low mass regions, respectively. The spectrum of the $m_{\mu^+\mu^-}$ invariant mass after the kinematic fit is shown in Figure 4 for the data at 189 GeV. A kinematic fit, assuming the lost electron along the beam line and no missing momentum in the transverse plane, was applied to improve the mass resolution.

The efficiency of the selection on the signal, the expected background and the number of selected events in the data at the two centre-of-mass energies are reported in Table 6 together with the evaluated cross-sections.

4.3 Systematic uncertainties

In both channels the main systematic uncertainty came from the limited simulation statistics available both for the signal and the background. As in the case of the single-W analysis the influence on the overall error is limited since the measurement is dominated by the real data statistics.

Besides this, in the hadronic channel two other sources of systematic errors were considered: the efficiency in the electron identification procedure and the limited knowledge

of the contribution from two-photon events which represents the largest background component.

The uncertainty on the efficiency of the electron identification was estimated by comparing the number of selected events in the data and in the simulation for a sample enriched in WW events with at least one of the two W's decaying, directly or in cascade, into a final state containing an electron. The same criteria for electron identification and isolation were adopted as in the Zee analysis. The relative difference in the efficiency was found to be $\Delta\varepsilon_e/\varepsilon_e = (6.7 \pm 8.2)\%$ where the error accounts both for the statistics and the systematics due to the presence of about 11% of background events in the selected sample. Conservatively, the error on the difference was used for the computation of the systematic error.

A $\pm 20\%$ uncertainty on the $\gamma\gamma$ background was assumed, as determined from a study on single tag events for both investigated final states.

The contributions of the different sources of systematics in the hadronic channel at 189 GeV are summarized in Table 8. The total systematic uncertainty amounts to $\pm 21\%$ in the region $15 < m_{q\bar{q}} < 60$ GeV/c^2 and to $\pm 13\%$ for $m_{q\bar{q}} > 60$ GeV/c^2.

The contributions of the different sources of systematics in the leptonic channel at 189 GeV are summarized in Table 9. The total systematic uncertainties amount to $\pm 22\%$ in the region $15 < m_{\mu^+\mu^-} < 60$ GeV/c^2 and to $\pm 9\%$ for $m_{\mu^+\mu^-} > 60$ GeV/c^2. For the measurement at 183 GeV, the same relative error was assumed.

5 Conclusions

The cross-sections for single-W production in the channels $e^-\bar{\nu}_e q\bar{q}'$ and $e^-\bar{\nu}_e l^+\nu_l$ ($l \neq e$) , assuming $\mu - \tau$ universality, have been measured in e^+e^- collisions at 182.6 and 188.6 GeV centre-of-mass energies by the DELPHI collaboration. These cross-sections have been determined within a restricted phase-space (see Section 2). The overall values are:

$$\sigma_{e\nu f\bar{f}'} = 0.49\ ^{+0.27}_{-0.22}\ (\text{stat.}) \pm 0.04\ (\text{syst.})\ \text{pb} \qquad (\sqrt{s} = 182.6\ \text{GeV}),$$

$$\sigma_{e\nu f\bar{f}'} = 0.45\ ^{+0.19}_{-0.16}\ (\text{stat.}) \pm 0.04\ (\text{syst.})\ \text{pb} \qquad (\sqrt{s} = 188.6\ \text{GeV}),$$

in agreement with the Standard Model expectations of 0.37 pb and 0.41 pb, respectively.

In addition, the cross-sections for $e^+e^- \to e\nu e\nu$, which include contributions both from single-W and from single-Z with a large interference between the two processes, have been measured to be:

$$\sigma(e^+e^- \to e\nu e\nu) = 0.024\ ^{+0.048}_{-0.024}\ (\text{stat.}) \pm 0.006\ (\text{syst.})\ \text{pb} \qquad (\sqrt{s} = 182.6\ \text{GeV}),$$

$$\sigma(e^+e^- \to e\nu e\nu) = 0.044\ ^{+0.031}_{-0.026}\ (\text{stat.}) \pm 0.011\ (\text{syst.})\ \text{pb} \qquad (\sqrt{s} = 188.6\ \text{GeV}),$$

in agreement with the Standard Model expectations of 0.041 pb and 0.046 pb, respectively. In both cases, the theoretical predictions have been computed with the GRC4F [6] and WPHACT [7] programs for the signal phase space defined in equations (1) and (3).

In the hadronic channel the cross-sections for single-Z production at $\sqrt{s} = 182.6$ GeV are:

$$\begin{aligned} \sigma &= 0.33\ ^{+0.28}_{-0.21}\ (\text{stat.}) \pm 0.08\ (\text{syst.})\ \text{pb} \quad 15 < m_{q\bar{q}} < 60\ \text{GeV}/c^2, \\ \sigma &= 1.66\ ^{+0.57}_{-0.48}\ (\text{stat.}) \pm 0.21\ (\text{syst.})\ \text{pb} \qquad m_{q\bar{q}} > 60\ \text{GeV}/c^2, \end{aligned}$$

and at $\sqrt{s} = 188.6$ GeV:

$$\sigma = 0.41\ ^{+0.16}_{-0.13}\ (\text{stat.}) \pm 0.09\ (\text{syst.})\ \text{pb} \quad 15 < m_{q\bar{q}} < 60\ \text{GeV}/c^2,$$
$$\sigma = 0.79\ ^{+0.23}_{-0.20}\ (\text{stat.}) \pm 0.10\ (\text{syst.})\ \text{pb} \quad m_{q\bar{q}} > 60\ \text{GeV}/c^2.$$

These values are found to be in agreement with Standard Model predictions, computed with GRC4F, which at $\sqrt{s} = 182.6$ GeV are:

$$\sigma = 0.45\ \text{pb} \quad 15 < m_{q\bar{q}} < 60\ \text{GeV}/c^2,$$
$$\sigma = 0.91\ \text{pb} \quad m_{q\bar{q}} > 60\ \text{GeV}/c^2,$$

and at $\sqrt{s} = 188.6$ GeV:

$$\sigma = 0.42\ \text{pb} \quad 15 < m_{q\bar{q}} < 60\ \text{GeV}/c^2,$$
$$\sigma = 0.94\ \text{pb} \quad m_{q\bar{q}} > 60\ \text{GeV}/c^2.$$

In the leptonic single-Z channel the cross-sections were determined at $\sqrt{s} = 188.6$ GeV only:

$$\sigma = 0.15\ ^{+0.21}_{-0.13}\ (\text{stat.}) \pm 0.03\ (\text{syst.})\ \text{pb} \quad 15 < m_{\mu^+\mu^-} < 60\ \text{GeV}/c^2,$$
$$\sigma = 0.08\ ^{+0.05}_{-0.04}\ (\text{stat.}) \pm 0.01\ (\text{syst.})\ \text{pb} \quad m_{\mu^+\mu^-} > 60\ \text{GeV}/c^2,$$

in agreement with the Standard Model predictions, computed with GRC4F:

$$\sigma = 0.112\ \text{pb} \quad 15 < m_{\mu^+\mu^-} < 60\ \text{GeV}/c^2,$$
$$\sigma = 0.033\ \text{pb} \quad m_{\mu^+\mu^-} > 60\ \text{GeV}/c^2.$$

6 Acknowledgements

We are greatly indebted to our technical collaborators, to the members of the CERN-SL Division for the excellent performance of the LEP collider and to the funding agencies for their support in building and operating the DELPHI detector.
We acknowledge in particular the support of
Austrian Federal Ministry of Education, Science and Culture, GZ 616.364/2-III/2a/98,
FNRS–FWO, Flanders Institute to encourage scientific and technological research in the industry (IWT), Belgium,
FINEP, CNPq, CAPES, FUJB and FAPERJ, Brazil,
Czech Ministry of Industry and Trade, GA CR 202/96/0450 and GA AVCR A1010521,
Commission of the European Communities (DG XII),
Direction des Sciences de la Matière, CEA, France,
Bundesministerium für Bildung, Wissenschaft, Forschung und Technologie, Germany,
General Secretariat for Research and Technology, Greece,
National Science Foundation (NWO) and Foundation for Research on Matter (FOM), The Netherlands,
Norwegian Research Council,
State Committee for Scientific Research, Poland, 2P03B06015, 2P03B11116 and SPUB/P03/DZ3/99,
JNICT–Junta Nacional de Investigação Científica e Tecnológica, Portugal,
Vedecka grantova agentura MS SR, Slovakia, Nr. 95/5195/134,
Ministry of Science and Technology of the Republic of Slovenia,
CICYT, Spain, AEN96–1661 and AEN96-1681,
The Swedish Natural Science Research Council,

Particle Physics and Astronomy Research Council, UK,
Department of Energy, USA, DE–FG02–94ER40817.

References

[1] DELPHI Collaboration, P. Abreu et al., Phys. Lett. **B459** (1999) 382.
[2] DELPHI Collaboration, P. Aarnio et al., Nucl. Instr. Meth. **A303** (1991) 253.
[3] DELPHI Collaboration, P. Abreu et al., Nucl. Instr. Meth. **A378** (1996) 57.
[4] P. Chochula et al., Nucl. Instr. Meth. **A412** (1998) 304.
[5] F. Boudjema et al., in *Physics at LEP2*, Vol.1, p. 228, G. Altarelli, T. Sjöstrand and F. Zwirner eds., CERN 96-01 (CERN, Geneva, 1996).
[6] J. Fujimoto et al., Comp. Phys. Comm. **100** (1997) 128.
[7] E. Accomando and A. Ballestrero, Comp. Phys. Comm. **99** (1997) 270.
[8] G. Altarelli, G. Martinelli, B. Mele and R. Ruckl, Nucl. Phys. **B262** (1985) 204;
E. Gabrielli, Mod. Phys. Lett. **A1** (1986) 465;
K. Hagiwara et al., Nucl. Phys. **B365** (1991) 544.
[9] F.A. Berends, R. Pittau and R. Kleiss, Comp. Phys. Comm. **85** (1995) 437.
[10] T. Sjöstrand, Comp. Phys. Comm. **39** (1986) 347; T. Sjöstrand, *PYTHIA 5.7 and JETSET 7.4 Physics and Manual*, CERN-TH/7112/93, revised August 1995.
[11] D. Karlen, Nucl. Phys. **B289** (1987) 23.
[12] S. Jadach, W. Placzeck and B.F.L Ward, Phys. Lett. **B390** (1997) 298.
[13] S. Jadach, B.F.L Ward and Z. Was, Comp. Phys. Comm. **79** (1994) 503.
[14] S. Nova, A. Olshevski and T. Todorov, CERN Yellow Report 2000-009.
[15] F.A. Berends, P.H. Daverveldt and R. Kleiss, Comp. Phys. Comm. **40** (1986) 271, 285, 309.
[16] ALEPH Collaboration, R. Barate et al., Phys. Lett. **B462** (1999) 389;
L3 Collaboration, M. Acciarri et al., Phys. Lett. **B487** (2000) 229.
[17] P. Abreu et al., Nucl. Instr. Meth. **A427** (1999) 487.
[18] S. Catani, *The k_T algorithm for jet production and fragmentation*, CERN-TH 6895/93 (1993).
[19] L. Lönnblad, Comp. Phys. Comm. **71** (1992) 15.
[20] OPAL Collaboration, G. Abbiendi et al., Phys. Lett. **B438** (1998) 391.

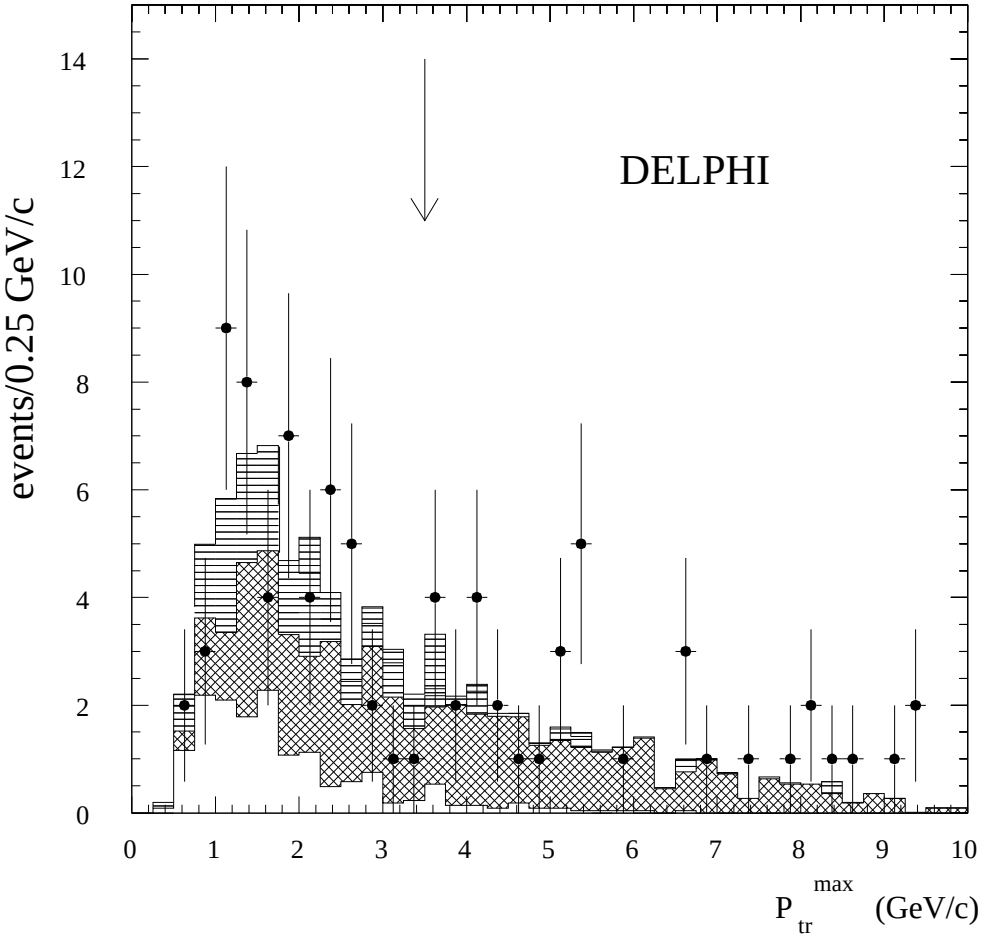

Figure 1: $e\nu_e W$ channel ($W \to q\bar{q}'$) at $\sqrt{s} = 189$ GeV. Maximum transverse momentum of any particle with respect to the closest jet. The open histogram represents the simulated $e^-\bar{\nu}_e q\bar{q}'$ signal, the cross-hatched area represents the WW background, the other backgrounds are shown with single hatching. Data points are indicated with statistical error bars. All the other selections described in Section 3.1 have already been applied. The arrow indicates the position of the cut on this variable.

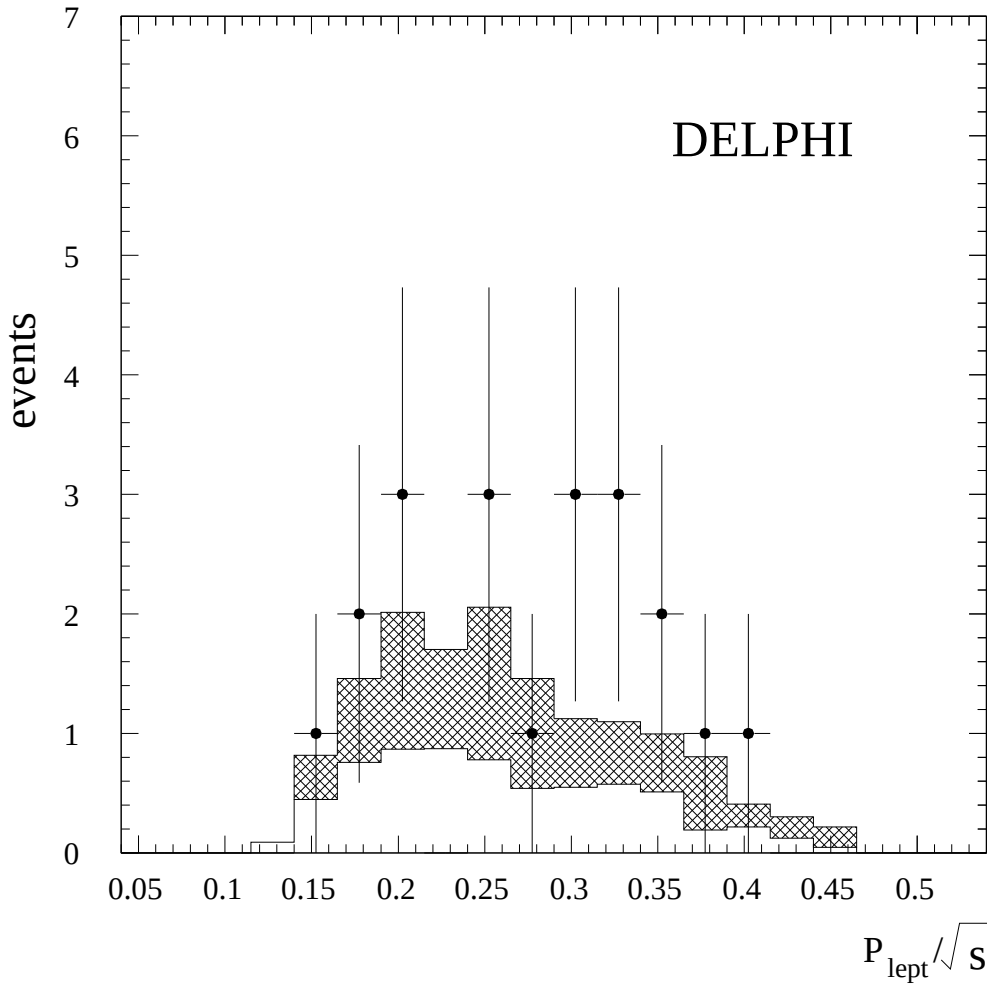

Figure 2: $e\nu_e W$ channel ($W \to l^+\nu_l$) at $\sqrt{s} = 189$ GeV. Momentum distributions of the lepton l^+ in real data (points with error bars) and in the simulation (histograms) for the events selected at the end of the analysis. The open area represents the single-W signal, the cross-hatched histogram is the background expectation.

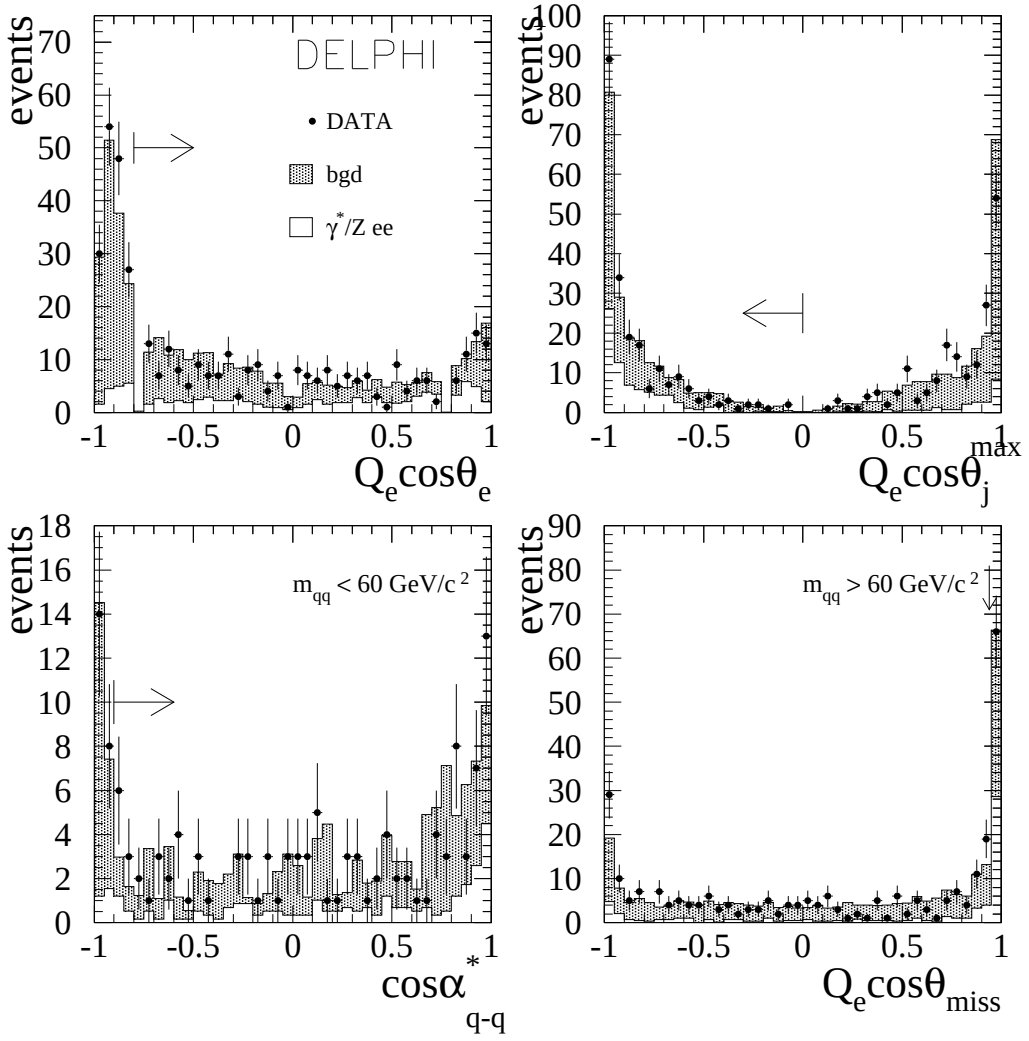

Figure 3: γ^*/Zee channel ($\gamma^*/Z \to q\bar{q}$) at $\sqrt{s} = 189$ GeV. Distributions of the variables used for the signal definition after the "electron identification" step (see Section 4.1), in real data (points with error bars) and in the simulation (histograms). The arrows indicate the value of the cut on each variable. The top plots show discriminant variables used for the signal selection in the overall $m_{q\bar{q}}$ spectrum. The bottom ones show the variables used for the different selections in the low (left) and high (right) invariant mass region of the hadronic system.

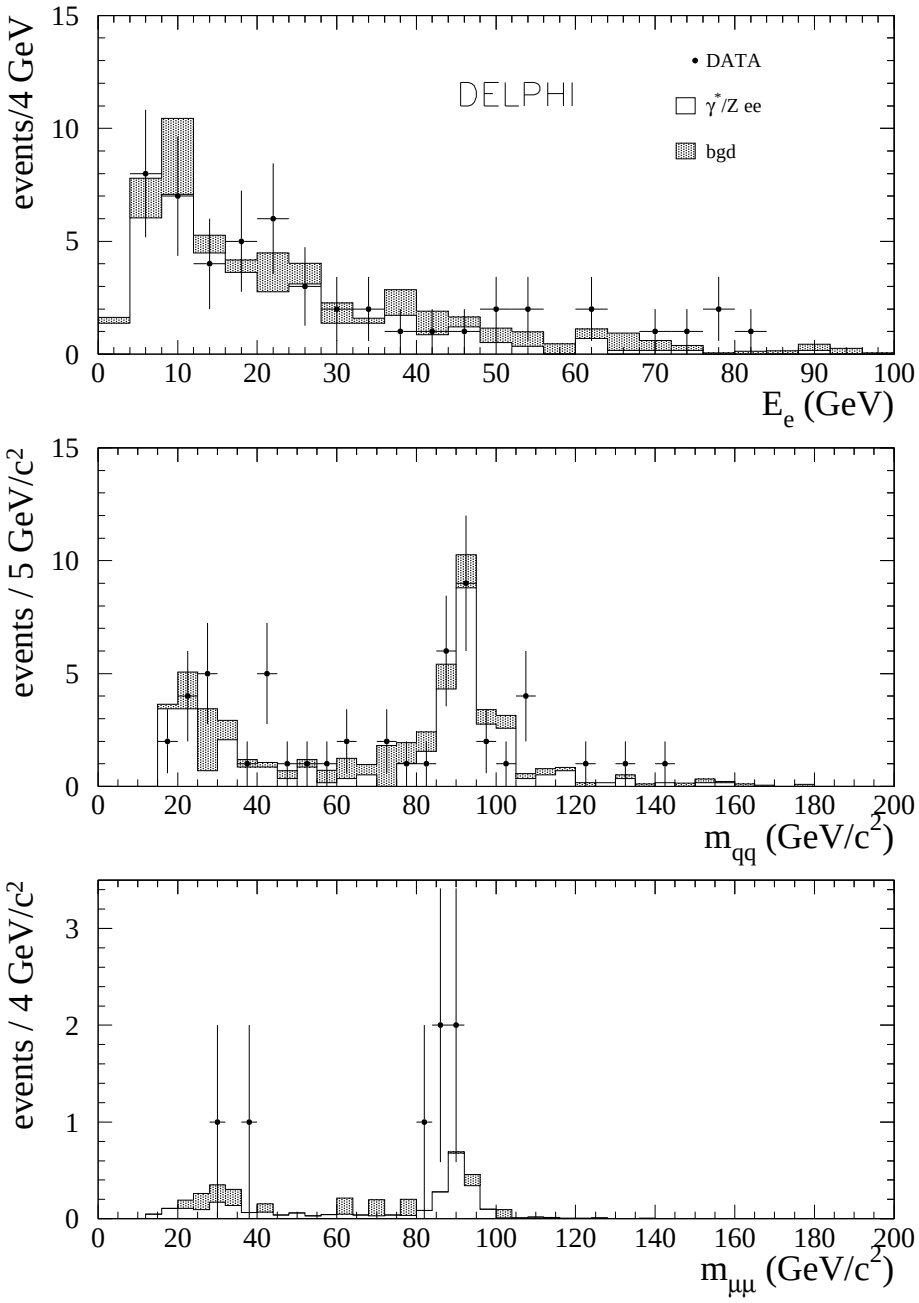

Figure 4: γ^*/Zee channel at $\sqrt{s} = 189$ GeV. Energy spectrum of the tag electron *(top)* and invariant mass distribution of γ^*/Z system *(centre)* in real data (points with error bars) and in the simulation (histograms) in the case of hadronic final states. Invariant mass distribution of the γ^*/Z system *(bottom)* in the case of $\mu^+\mu^-$ final states.